



ULUSLARARASI 3B YAZICI TEKNOLOJİLERİ
VE DİJİTAL ENDÜSTRİ DERGİSİ

INTERNATIONAL JOURNAL OF 3D PRINTING
TECHNOLOGIES AND DIGITAL INDUSTRY

ISSN:2602-3350 (Online)

URL: <https://dergipark.org.tr/ij3dptdi>

EFFECTS OF POSITIONING CONDITIONS ON MATERIAL PROPERTIES IN POWDER BED FUSION ADDITIVE MANUFACTURING

Yazarlar (Authors): Mevlüt Yunus Kayacan^{ID*}, Nihat Yılmaz^{ID}

Bu makaleye şu şekilde atıfta bulunabilirsiniz (To cite to this article): Kayacan M. Y., Yılmaz N., "Effects of Positioning Conditions On Material Properties In Powder Bed Fusion Additive Manufacturing" *Int. J. of 3D Printing Tech. Dig. Ind.*, 6(2): 218-227, (2022).

DOI: 10.46519/ij3dptdi.1098368

Araştırma Makale/ Research Article

Erişim Linki: (To link to this article): <https://dergipark.org.tr/en/pub/ij3dptdi/archive>

EFFECTS OF POSITIONING CONDITIONS ON MATERIAL PROPERTIES IN POWDER BED FUSION ADDITIVE MANUFACTURING

Mevlüt Yunus Kayacan^a *, Nihat Yılmaz^a 

^aIsparta University of Applied Sciences, Mechanical Engineering, Isparta, TURKEY

* Sorumlu Yazar: mevlutkayacan@isparta.edu.tr

(Received: 04.04.2022; Revised: 13.05.2022; Accepted: 15.07.2022)

ABSTRACT

Among additive manufacturing technologies, Powder Bed Fusion (PBF) is considered the most common process. Although the PBF has many advantages, some issues need to be clarified, such as positioning. In this study, the effect of positioning on the microstructures in the PBF method was investigated. Ti6Al4V samples were manufactured in different positions on the building platform and investigated by means of temperature, porosity, microstructure and hardness. In this study, martensitic needles were detected on the microstructure samples. Some twins were noticed on primary martensitic lines and the agglomeration of β precipitates was observed in vanadium-rich areas. The positioning of samples were revealed to have an effect on temperature gradients and the average martensitic line dimensions. Besides, different hardness values were attained depending on sample positioning conditions. As a major result, cooling rates were found related to the positions of samples and the location of points on the samples.

Keywords: Additive Manufacturing, Selective Laser Melting, Ti6Al4V, Thermal Effect, Temperature Distribution.

1. INTRODUCTION

Additive manufacturing (AM) processes are considered game-changer in the industrial field due to their ability to produce complex geometries without waste of feedstock material [1]. In particular, Powder Bed Fusion additive manufacturing technologies, which includes selective laser melting (SLM) and electron beam melting, are used to manufacture prototypes and small series of metallic complex parts [2]. In the SLM process a wide range of materials is available for many applications and novel materials can be developed for specific applications [3]. SLM technique comprised many advantages such as complex-shaped, light weighted and custom-made part manufacturing; nevertheless, some issues like hot cracks, residual stresses, porosities and lack-of-fusion defects can be present in SLM parts [4]. Lack of fusion defects occurred due to inadequate laser energy density. To prevent this defect, the energy concentration must be tuned by changing the manufacturing parameters [5]. The heating of the building platform is

generally performed to decrease thermal stresses and reduce the formation of hot cracks within the material microstructure [6]. The relation between thermal gradient and residual stress was revealed by experimental methods and finite element analysis in ref. [7, 8].

Different thermal histories can lead to substantial differences in terms of microstructural and mechanical properties of the final component [9]. Estimating and controlling the microstructure of the processed material would be beneficial to achieve enhanced mechanical properties [10]. Many parameters such as laser speed, energy density, layer thickness and hatch distance affect the microstructure of materials during SLM process. Furthermore, some extra parameters that affect material microstructure should be considered, including orientation and position of components on the building platform and temperature distribution [11].

Ti6Al4V is widely used for additive manufacturing of components that are employed in medical and aerospace industries

due to its lightness, biocompatibility and good compromised of mechanical properties [13]. Several studies regarding the effect of manufacturing parameters on Ti6Al4V microstructure were published [14, 15]. Parameter optimization was accomplished to obtain small grains and homogenous microstructures [16]. Numerous studies addressed the investigation of microstructural defects such as cracks, and lack of fusion pores [17]. Grains of α' -phase and acicular martensite needles were found within the microstructure of T6Al4V produced by SLM [18]. As the cooling rate increases, the microstructure shows a higher quantity of martensite, leading to an embrittlement of the material [12]. In addition to that, some of the thermal situations could cause differences in the microstructures. In particular, higher grades of additional martensitic lines, dislocations, and twins emerged [19]. Prior researches have emphasized that twins, which were, restrained the elongation of martensitic lines and lead to precipitation of fine grains, lead to increased mechanical properties. Furthermore, secondary martensite lines affected the mechanical properties of materials as well. Some authors have driven the further development of the additive manufacturing of Ti6Al4V considering the effect of process temperatures and cooling rates on the final microstructure. The complexity of the microstructure consisted of a large martensitic lines, arising of secondary, ternary and quaternary martensitic lines, dislocations and twins [20, 21].

In the literature, besides microstructure of SLM additive manufactured Ti6Al4V material was examined many times, there was no study about manufacturing of multiple samples at the same time. Positioning-related microstructures were not focused on before in the articles. In this study, samples of Ti6Al4V were produced by SLM placed in different positions on the building platform in order to evaluate the effect of temperature distribution and cooling rate on the microstructure and porosity of the material. Moreover, the effect of different microstructure on the final hardness of samples was evaluated.

2. MATERIALS AND METHODS

The chemical composition of the gas-atomized Ti6Al4V powder is reported in Table 1.

Table 1. Chemical composition of Ti6Al4V.

Material	% by weight
Titanium	89.7
Aluminum	5.9
Vanadium	4.2
Iron	0.1
Oxygen	0.1

A EOS M280 DMLS system was used to produce 5 cubic samples using the gas-atomized Ti6Al4V powder. In the study, results were interpreted clearly with the production of 5 samples representing different positions. With the manufacturing of samples larger than 5 mm, the inadequacy of mechanical properties and problems in the microstructure have been largely avoided. The mechanical properties increase with increasing sample size [22,23]. The majority of prior researchers have found that the optimum parameters were defined as 1250 mm/s scanning speed, 170 W laser power, 0.7 mm hatching distance, 0.03 mm layer thickness, 67° rotational scanning, and 50.7 J/mm³ energy density [24]. Ti6Al4V gas atomized powder from EOS GmbH was used in the present study. The morphology of the powder particles was spherical in shape. However, several satellites are attached to the powder particles. The average diameter of the powder particles is observed to be $36 \pm 5 \mu\text{m}$ [25]. Purity of argon gas was 99.999% to guarantee a controlled atmosphere during the process. The cubic samples were sized as 10x10x10 mm³. The distance between cubes was 5 mm. The distribution of the samples on the building platform is depicted in Fig. 1. Besides, 2 mm block type support structures were implemented. Manufactured samples were cut from the build platform by wire electrical discharge machine.

The temperature of molten materials was found by the experimentally validated thermal camera measurements. Curves of temperature were achieved by Optris PI160 thermal camera system with 120 Hz frequency. The camera system was installed at the top surface of the manufacturing cabin to focus on the manufacturing platform. The camera recorded videos from 350 mm far away from the build platform at 14°. The emissivity value of Ti6Al4V material was experimentally defined between 0.31 and 0.38 depending on the temperature. The manufactured samples were cut to analyze two sections (top and middle,

respectively) as reported in Fig. 1c. The relative density investigation and measurement of martensite lath width were carried out through image processing by using Image J software. ImageJ software was used to investigate the relative density values. Microstructure analysis was carried out by Nikon Eclipse LV150NL light optical microscope (LOM) and by Zeiss Sigma 500 field emission scanning electron

microscope (FE-SEM) equipped with Oxford Instruments Ultim Max detector for energy dispersive X-ray analysis (EDS). Leica Mod VMHT 30 tester was used to evaluate the hardness of samples. A load of 100g and a dwell time of 15 seconds were used to perform hardness tests according to the ASTM E92-17 standard [26].

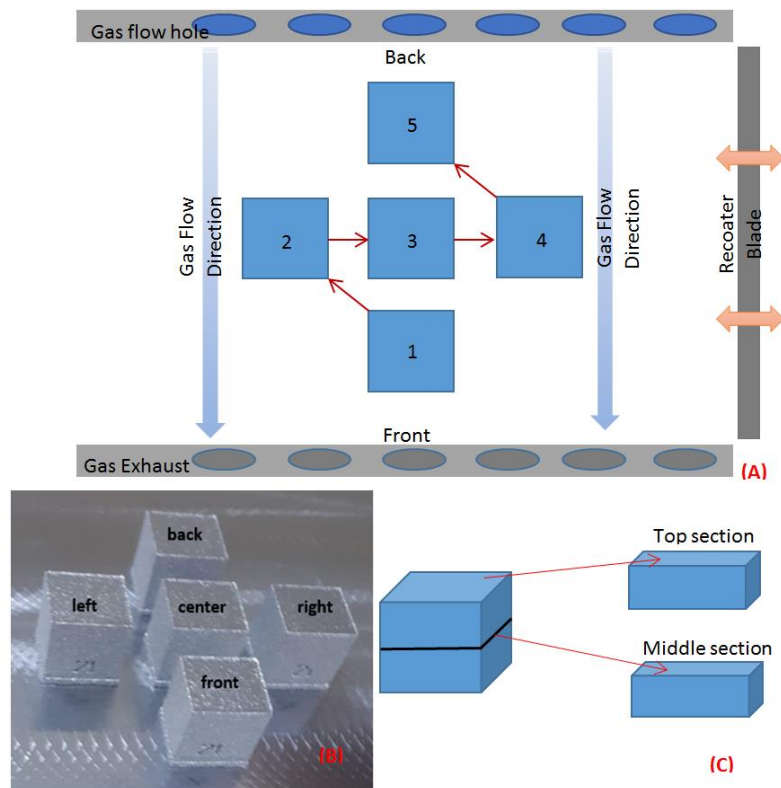


Figure 3. 1 A. Schematic of position of samples on building platform; B. Photo of manufactured samples; C. Schematic of analyzed sections

3. RESULTS AND DISCUSSIONS

The maximum temperature values of the top and middle sections of each sample are shown in Fig 2. The maximum temperature value increases from the middle to the top section for every investigated sample, indicating that the material experiences a heat accumulation during the manufacturing process. The accumulation phenomenon was particularly

evident on sample 3, probably due to its proximity to other samples and limited heat transfer condition (Fig. 1). Moreover, heat transfer mechanism, geometry and positioning of samples have a strong influence on the temperature gradients experienced by the material. [27, 28]. Temperature values obtained by the thermal camera were consistent with the literature [29].

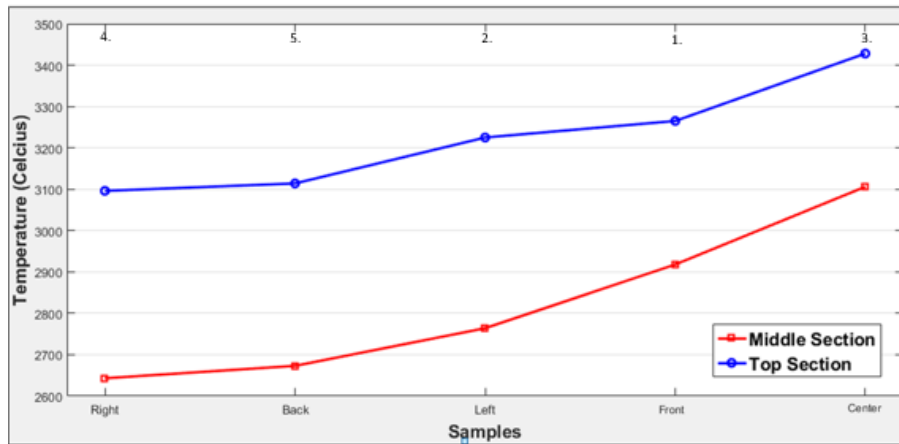


Figure 2. Peak temperatures on manufactured samples

The sections of samples parallel to the building platform were investigated by optical microscope in order to perform relative density analysis. The relative density values of samples were reported in Fig. 3 and range between 99.98% and 99.95%. These results were similar to the literature [30]. Mean Standard deviation

of the results was found as 0.005%. Higher maximum temperature values can promote the formation of a larger quantity of sputters, exhaust gasses and residues of burnt materials during the laser scan [31-34]. These phenomena can also cause increased porosity.

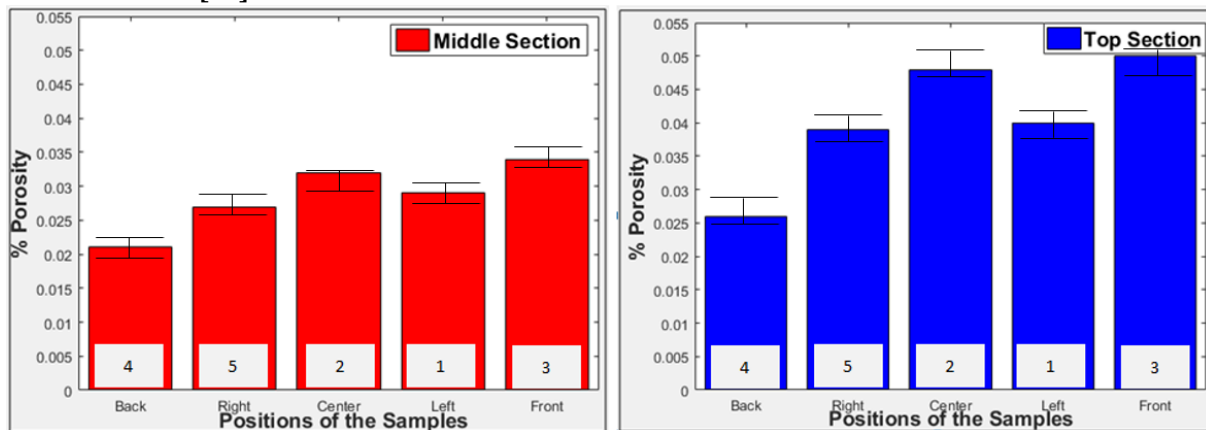


Figure 3. Porosity ratio of samples with regard to positions

The section of as-built samples parallel to the building platform was etched by Kroll's reagent and investigated by optical and SEM microscopes. Surfaces of the samples were observed with 50x and 200x OM magnification,

as reported in Fig. 4. The martensitic α' phase is noticeable within the microstructure of all investigated sections, in good agreement with literature results [35, 36].

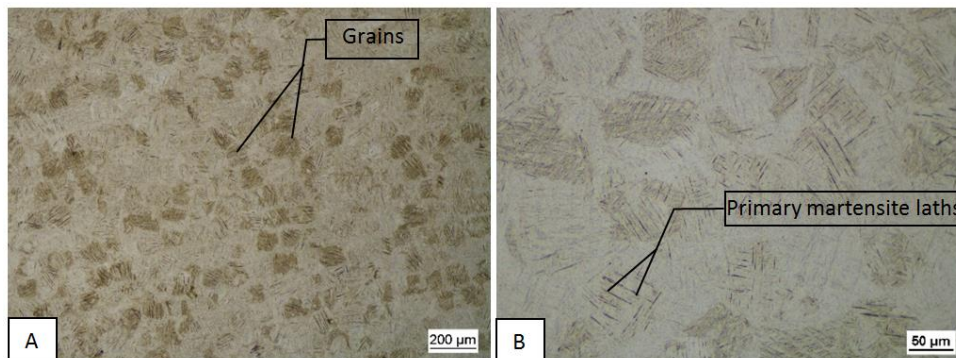


Figure 4. A) Low-magnification and B) high-magnification optical images of the section parallel to the building platform of as-built samples

Results were reported in Fig. 5. Martensitic laths with different thicknesses are visible within the microstructure of the as-built material. Thin martensitic laths were recognized on the top surface of the samples (Fig.5A-B), while thick martensitic laths were observed in the middle section (Fig.5C-D). It was thought that the higher maximum temperature values achieved in the top section as seen (Fig. 2). This could lead to lower cooling rates due to lower temperature gradient, which was related to cooling through the melting temperature to mean layer temperature. Mean layer temperature increased during manufacturing from 35°C to 75°C. It was

occurred owing to more effectual repetitive laser heating and cooling cycle in the middle section than the top section. Similar to this study, it was found that primary and secondary α' martensites were a little coarsening, while the finer ternary and quartic martensite laths were forming [21]. The High magnification SEM images are shown in Fig 6. Similar in the literature, twins were seen on the primary martensitic laths. Besides, primary, secondary and ternary α' martensitic laths were ascertained in the as-built microstructure. Thermal history induced severe internal stresses caused dislocations such as twins.

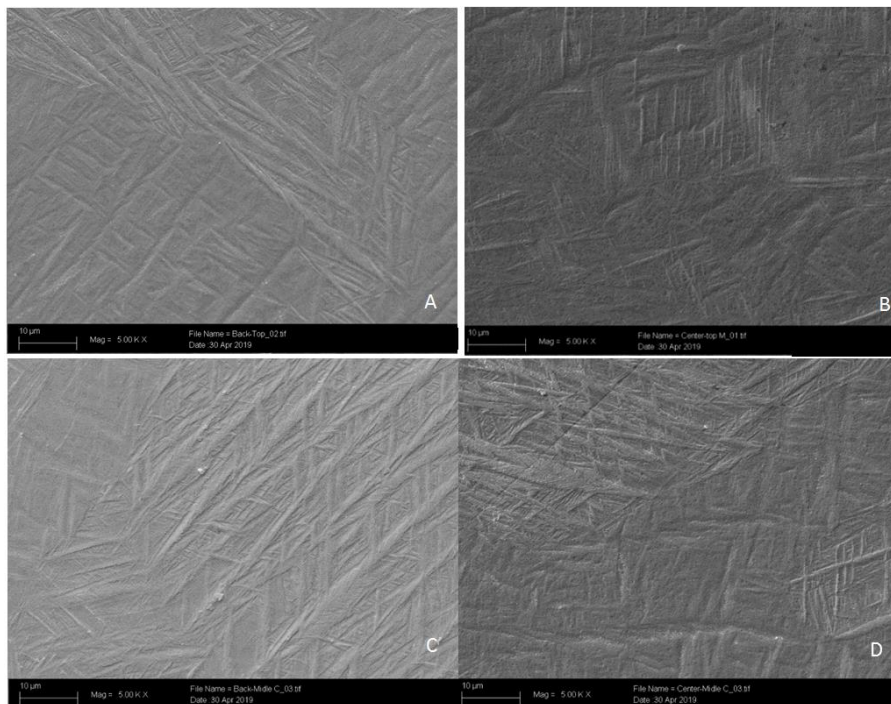


Figure 5. SEM images of Back sample, top surface (A), Center sample, top surface (B), Back sample, middle surface (C), Center sample, middle surface (D)

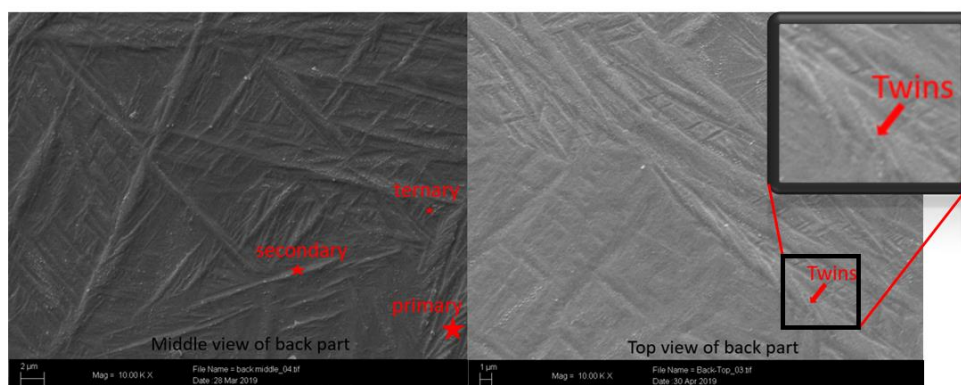


Figure 6. Twins and additional martensitic lines in α' phase

SEM images reported in Fig. 7 shows the evidence of white spots within the microstructure of the as-built material. These spots were ascribed to the β phase, related to agglomerations of vanadium atoms as observed with EDX analysis. Vanadium content was 4.9% in the material and 0.7% more than the standard. The β phase can appear in form of white spots due to the higher vanadium content that results in a brighter contrast [37, 38]. The zone of Fig.7-A showed the more brittle and harder mechanical properties.

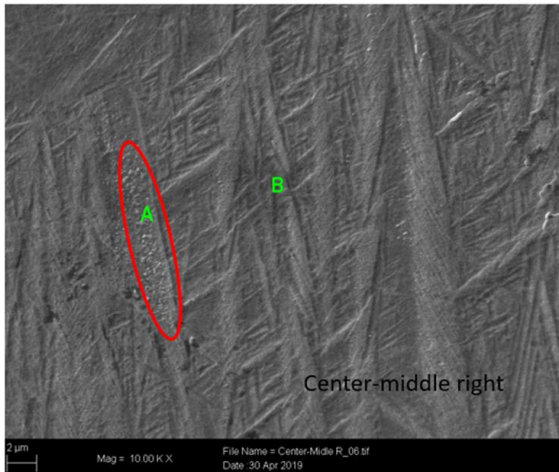


Figure 7. Agglomeration of β precipitates in the α' martensitic phase

Finally, the widths of primary martensitic laths were measured in order to understand the influence of the building position and maximum temperature of samples on the final microstructure. Results were reported in Fig 8. The widths of martensitic lines were measured on 7 different laths with SEM images. Mean standard deviation of the measurements was calculated as $\pm 0.135 \mu\text{m}$. Thinner martensitic laths are visible on top sections of both center and back samples. The samples, which are placed nearby the argon gas inlet, were cooled faster according to temperature values of samples (Fig. 2). Thus the maximum temperature results observed higher far samples from the gas inlet. This phenomenon led to emerging thinner martensitic lines on neighboring fields to argon gas flow due to lower temperature gradient. While coarser primary martensite laths were formed, finer grains were existed due to forming secondary, tertiary and quartic martensite laths. Besides, in nearby areas such as edges and corners of two adjacent samples, secondary heat effects were noticed by analyzing the width of martensitic lines according to the observations in Fig 5.

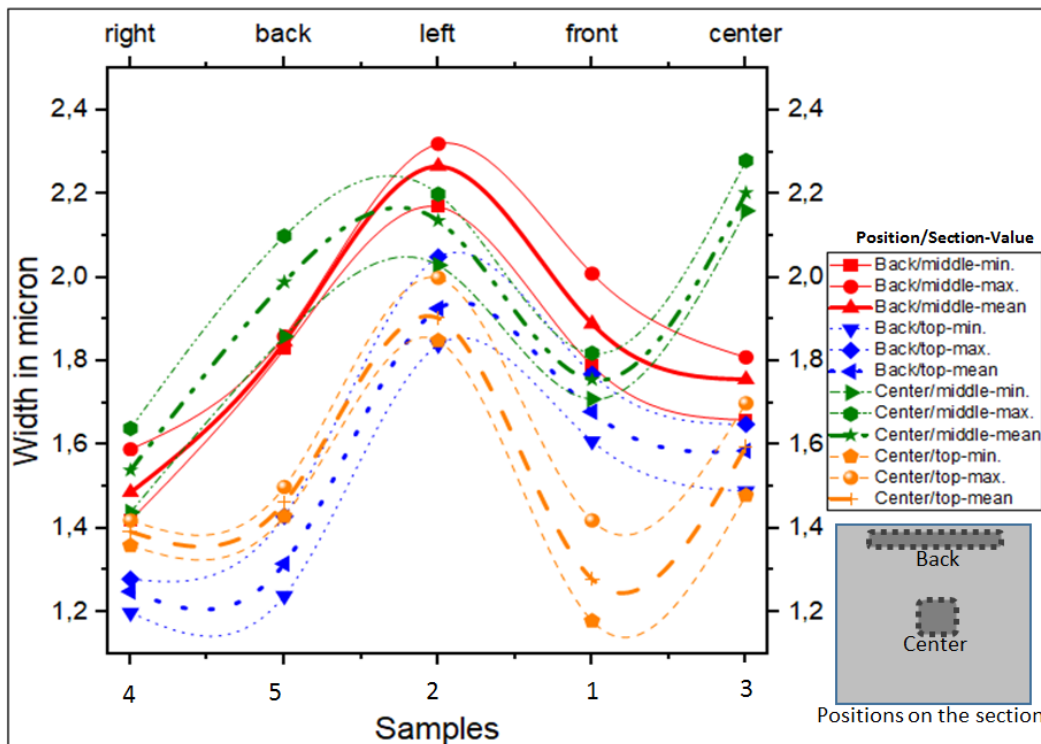


Figure 8. Primary martensitic lath width for different sections of samples

Micro hardness values of the center point of samples were shown in Fig 9. Top section of the samples shows lower micro-hardness values than those of middle sections, probably due to the complexity (further α phase transformations) of the microstructures. Although the primary martensitic lath width of the top section was finer, additional martensitic lines (finer than the primary martensitic lath) on the middle section led microstructure to more complex than the top section. Though the primary martensitic laths of the middle areas were larger than the top areas, middle areas were observed more complex than the top areas in the light of figures 5 and 6. Significantly, lower hardness values were noticed on sample 3 than sample 5 due to coarser laths. In the literature, similar results were taken that The

width of the acicular α' martensite increased and the length decreased with an increasing number of melting steps from single to triple melting. Since the position of the back sample is closer to the gas the material, leading to higher micro-hardness values, can experience inlet, higher cooling rate. Accordingly, the hardness on edges and corners were ranged between 365-400 HV and micro hardness values at the center points varied between 390-400 HV. The results were similar with previous studies wherein the hardness of the Ti6Al4V material in PBF additive manufacturing was measured between 330-407 HV. With the repetitive and high energy density melting process, the structure of the α' martensite phases changed and the hardness increased [39, 40].

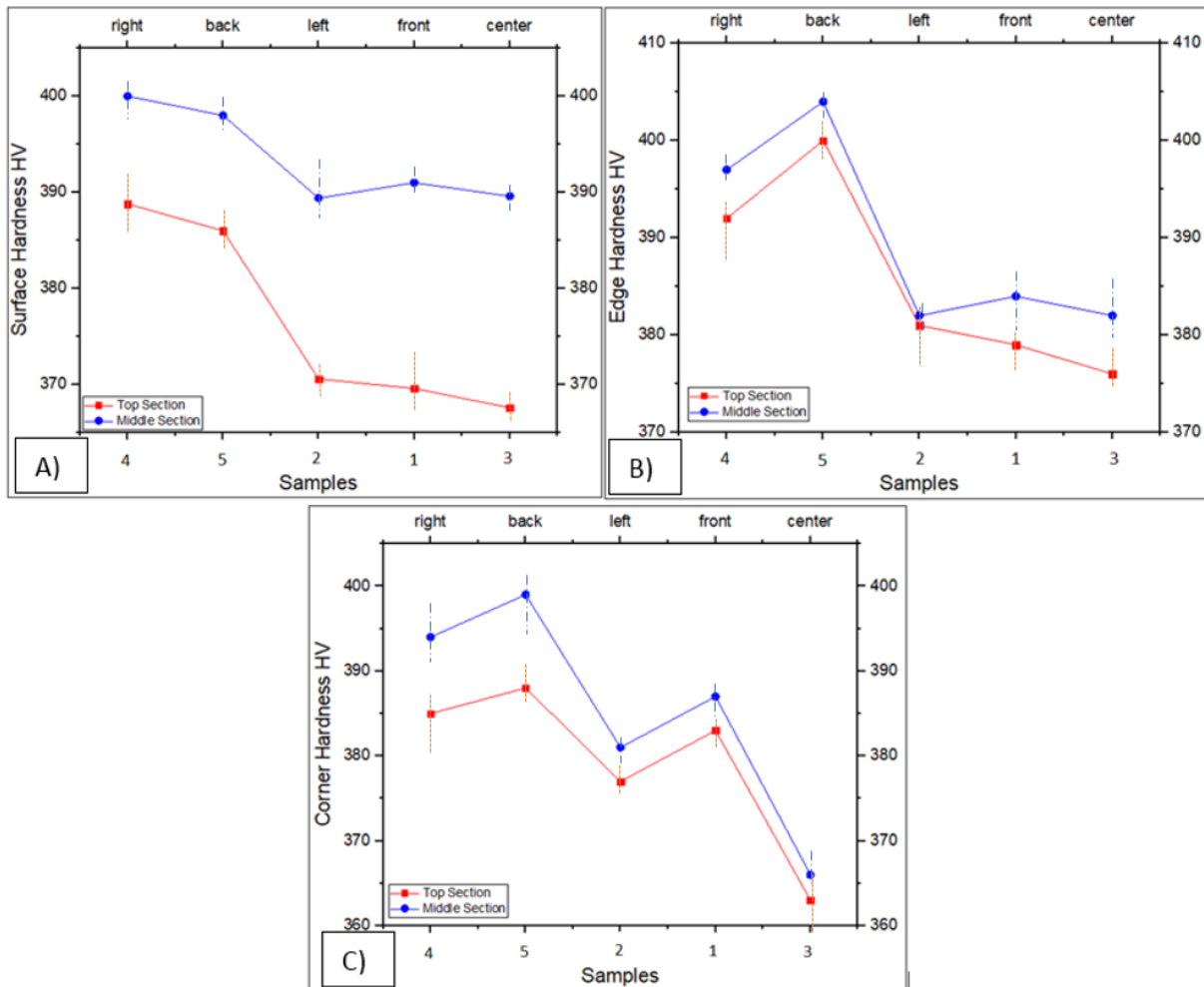


Figure 9. A) Micro hardness values of center point of samples, B) Micro hardness values of edge of samples, C) Micro hardness values of corner of samples

Mean standard deviations of micro hardness values were found as ± 9.75 HV. According to previous results, the micro-hardness of samples

fluctuates depending on the section and position of the samples on the building platform. Side surfaces, edges and corners were adequate

owing to the resistance to friction, internal/residual stresses and deformations. Nevertheless, in case of the reaching excessive hardness, outer surfaces would be brittle. Therefore, unexpected failure mechanisms could be occurred.

4. CONCLUSIONS

In this study, the effects of positioning of samples on the manufacturing platform were investigated by various methods. Remarkable results were identified as seen below.

- Some residues and exhaust gasses came in sight during the melting powders by the laser. Some additional constituents in the powders were burned and the residues which came up by the melting process were relocated to the sample 1 owing to the argon gas flow. Hence, the sample 1 was affected negatively and had a high porosity rate more than the others.
- Temperatures of all samples were linearly increased during manufacturing. The temperature gradient on the samples was not homogenous due to their positions on the building platform. Remarkably, the temperature on sample 3, located at the center of the platform, had higher temperature values and lower temperature gradient than the others. Sample 3 had boundary conditions that made heat transfer difficult due to being surrounded by other samples.
- The top section of samples showed thinner primary martensitic lines than the middle (inner) section but also the minimum primary martensitic line widths of the middle section were thinner than top section. The middle section of samples included secondary and ternary numerous sub-martensitic lines more than the top section. Furthermore, the center of the samples included thicker martensitic lines than side areas. As the laser melting the upper layers, previous layers were influenced. Further, heat performs like heat treatment upon the material. Upper layers of samples had fewer complex microstructures.
- The most significant differences in temperature and hardness were noticed between the sample 3 and 5 since the higher cooling rate was observed on the back sample due to its closer position to gas flow hole. Higher cooling rates prompted to

acquire harder samples because of martensitic transformation. Middle sections of samples had higher hardness values than the top section due to the complexity of α' phases and it was associated with multiple quenching of the material.

ACKNOWLEDGES

This work was completed without any funding or support.

REFERENCES

1. Kayacan M.C., Delikanli Y.E., Duman B., Ozsoy K., "Examining of mechanical properties of transitive (variable) porous specimens produced by SLS using ti6Al4v alloy powder", Journal of the Faculty of Engineering and Architecture of Gazi University, Vol. 33, Issue 1, Pages 127-143, 2018.
2. Badiru A.B, Valencia V.V., Liu D., "Additive manufacturing handbook: product development for the defense industry". CRC Press, 2017.
3. Poprawe R, Hinke C., Meiners W., Schrage J., Bremen S., Merkt S., "SLM production systems: recent developments in process development, machine concepts and component design" Advances in Production Technology, Pages 49-65, 2015.
4. Patterson A.E., Messimer S.L., Farrington P.A., "Overhanging features and the SLM/DMLS residual stresses problem: Review and future research need" Technologies, Vol. 5, Issue 2, Page 15, 2017.
5. Arısoy Y.M, Ciales, L.E, Özel T., Lane B., Moylan S., Donmez A., "Influence of scan strategy and process parameters on microstructure and its optimization in additively manufactured nickel alloy 625 via laser powder bed fusion" The International Journal of Advanced Manufacturing Technology, Vol. 90, Issue 5-8, Pages 1393-1417, 2017.
6. Zhao C., Fezzaa K., Cunningham R.W., Wen H., De Carlo F., Chen L., Sun T., "Real-time monitoring of laser powder bed fusion process using high-speed X-ray imaging and diffraction" Scientific reports, Vol. 7, Issue 1, Pages 1-11, 2017.
7. Ali H., Ma L., Ghadbeigi H., Mumtaz K., "In-situ residual stress reduction, martensitic decomposition and mechanical properties enhancement through high temperature powder bed pre-heating of Selective Laser Melted Ti6Al4V". Materials Science and Engineering: A, Vol. 695, Pages 211-220, 2017.

8. Li C., Liu Z.Y., Fang X.Y., Guo Y.B., "Residual stress in metal additive manufacturing" *Procedia CIRP*, Vol. 71, Pages 348-353, 2018.
9. Acharya R., Sharon J.A., Staroselsky A., "Prediction of microstructure in laser powder bed fusion process" *Acta Materialia*, Vol. 124, Pages 360-371, 2017.
10. Murr L.E., Quinones S.A., Gaytan S.M., Lopez M.I., Rodela A., Martinez E.Y., Wicker R.B., "Microstructure and mechanical behavior of Ti-6Al-4V produced by rapid-layer manufacturing, for biomedical applications" *Journal of the mechanical behavior of biomedical materials*, Vol. 12, Issue 1, Pages 20-32, 2009.
11. Song B., Dong S., Zhang B., Liao H., Coddet, C. "Effects of processing parameters on microstructure and mechanical property of selective laser melted Ti6Al4V" *Materials & Design*, Vol. 35, Pages 120-125, 2012.
12. Scharowsky T., Juechter V., Singer R.F., Körner C., "Influence of the scanning strategy on the microstructure and mechanical properties in selective electron beam melting of Ti-6Al-4V" *Advanced Engineering Materials*, Vol. 17, Issue 11, Pages 1573-1578, 2015.
13. Yadroitsev I., Krakhmalev, P., Yadroitsava I., Du Plessis A., "Qualification of Ti6Al4V ELI alloy produced by laser powder bed fusion for biomedical applications". *JOM*, Vol. 70, Issue 3, Pages 372-377, 2018.
14. Yadroitsev I., Krakhmalev P., Yadroitsava I., "Selective laser melting of Ti6Al4V alloy for biomedical applications: Temperature monitoring and microstructural evolution" *Journal of Alloys and Compounds*, Vol. 583, Pages 404-409, 2014.
15. Rafi H.K., Karthik N.V., Gong H., Starr T.L., Stucker B.E., "Microstructures and mechanical properties of Ti6Al4V parts fabricated by selective laser melting and electron beam melting". *Journal of materials engineering and performance*, Vol. 22, Issue 12, Pages 3872-3883, 2013.
16. Shipley H., McDonnell D., Culleton M., Coull R., Lupoi R., O'Donnell G., Trimble, D., "Optimisation of process parameters to address fundamental challenges during selective laser melting of Ti-6Al-4V: A review" *International Journal of Machine Tools and Manufacture*, Vol. 128, Pages 1-20, 2018.
17. Galarraga H., Lados D.A., Dehoff R.R., Kirka M.M., Nandwana, P., "Effects of the microstructure and porosity on properties of Ti-6Al-4V ELI alloy fabricated by electron beam melting (EBM)" *Additive Manufacturing*, Vol. 10, Pages 47-57, 2016.
18. Yadroitsev I., Krakhmalev P., Yadroitsava I., "Selective laser melting of Ti6Al4V alloy for biomedical applications: Temperature monitoring and microstructural evolution" *Journal of Alloys and Compounds*, 583 404-409, 2014.
19. Vrancken B., Thijs L., Kruth J.P., Van Humbeeck J., "Heat treatment of Ti6Al4V produced by Selective Laser Melting: Microstructure and mechanical properties" *Journal of Alloys and Compounds*, Vol. 541, Pages 177-185, 2012.
20. Cao S., Chen Z., Lim C.V.S, Yang K., Jia Q., Jarvis T., Wu X., "Defect, microstructure, and mechanical property of Ti-6Al-4V alloy fabricated by high-power selective laser melting" *JOM*, Vol. 69, Issue 12, Pages 2684-2692, 2017.
21. Yang J., Yu H., Yin J., Gao M., Wang Z., Zeng X., "Formation and control of martensite in Ti-6Al-4V alloy produced by selective laser melting" *Materials & Design*, Vol. 10, Pages 308-318, 2016.
22. Karimi J., Suryanarayana C., Okulov I., Prashanth K.G., "Selective laser melting of Ti6Al4V: Effect of laser re-melting" *Materials Science and Engineering: A*, Vol. 805, Issue 140558, 2021.
23. Phutela C., Aboulkhair N.T., Tuck C.J., Ashcroft I., "The effects of feature sizes in selectively laser melted Ti-6Al-4V parts on the validity of optimised process parameters" *Materials*, Vol. 13, Issue 1, Page 117, 2020.
24. Kayacan M.C., Delikanlı Y.E., Duman B., Özsoy K., "Ti6Al4V toz alaşımı kullanılarak SLS ile üretilen geçişli (değişken) gözenekli numunelerin mekanik özelliklerinin incelenmesi" *Gazi Üniversitesi Mühendislik-Mimarlık Fakültesi Dergisi*, Vol. 33, Issue 1, 2018.
25. Rafi H.K., Karthik N.V., Gong H., Starr T.L., Stucker B.E., "Microstructures and mechanical properties of Ti6Al4V parts fabricated by selective laser melting and electron beam melting" *Journal of materials engineering and performance*, Vol. 22, Issue 12, Pages 3872-3883, 2013.
26. ASTM E92-17: Standard test methods Standard Test Methods for Vickers Hardness and Knoop Hardness of Metallic Materials.
27. Dunbar A.J., Denlinger E.R., Gouge M.F., Simpson T.W., Michaleris P., "Comparisons of laser

powder bed fusion additive manufacturing builds through experimental in situ distortion and temperature measurements” Additive Manufacturing, Vol. 15, Pages 57-65, 2017.

28. Criales L.E., Özel T., “Temperature profile and melt depth in laser powder bed fusion of Ti-6Al-4V titanium alloy” Progress in Additive Manufacturing, Vol. 2, Issue 3, Pages 169-177, 2017.

29. Zhuang J.R., Lee Y.T., Hsieh W.H., Yang A.S., “Determination of melt pool dimensions using DOE-FEM and RSM with process window during SLM of Ti6Al4V powder” Optics & Laser Technology, Vol. 103, Pages 59-76, 2018.

30. Van Hooreweder B., Moens D., Boonen R., Kruth J.P., Sas P., “Analysis of fracture toughness and crack propagation of Ti6Al4V produced by selective laser melting” Advanced Engineering Materials, Vol. 14, Issue 1-2, Pages 92-97, 2012.

31. Shutov I.V., Gordeev G.A., Kharanzhevskiy E.V., Krivilyov M.D., “Analysis of morphology and residual porosity in selective laser melting of Fe powders using single track experiments” IOP Conference Series: Materials Science and Engineering, Vol. 192, 2017.

32. Ferrar B., Mullen L., Jones E., Stam R., Sutcliffe C.J., “Gas flow effects on selective laser melting (SLM) manufacturing performance” Journal of Materials Processing Technology, Vol. 21, Issue 2, Pages 355-364, 2012.

33. Fousová M., Vojtěch D., Kubásek J., Jablonská E., Fojt J., “Promising characteristics of gradient porosity Ti-6Al-4V alloy prepared by SLM process” Journal of the mechanical behavior of biomedical materials, Vol. 69, Pages 368-376, 2017.

34. Kasperovich G., Haubrich J., Gussone J., Requena G., “Correlation between porosity and processing parameters in TiAl6V4 produced by selective laser melting” Materials & Design, Vol. 105, Pages 160-170, 2016.

35. Vrancken B., Thijs L., Kruth J.P., Van Humbeeck J., “Heat treatment of Ti6Al4V produced by Selective Laser Melting: Microstructure and mechanical properties” Journal of Alloys and Compounds, Vol. 541, Pages 177-185, 2012.

36. Thijs L., Verhaeghe F., Craeghs T., Van Humbeeck J., Kruth J.P., “A study of the microstructural evolution during selective laser melting of Ti-6Al-4V”. Acta materialia, Vol. 58, Issue 9, Pages 3303-3312, 2010.

37. Agius D., Kourousis K.I., Wallbrink C., Song T., “Cyclic plasticity and microstructure of as-built SLM Ti-6Al-4V: The effect of build orientation” Materials Science and Engineering: A, Vol. 70185, Issue 100, 2017.

38. Tao P., Li H.X., Huang B.Y., Hu Q.D., Gong S.L., Xu Q.Y., “Tensile behavior of Ti-6Al-4V alloy fabricated by selective laser melting: Effects of microstructures and as-built surface quality” China Foundry, Vol. 15, Issue 4, Pages 243-252, 2018.

39. Khorasani A., Gibson I., Awan U.S., Ghaderi A., “The effect of SLM process parameters on density, hardness, tensile strength and surface quality of Ti-6Al-4V” Additive Manufacturing, Vol. 25, Pages 176-186, 2019.

40. Wang D., Dou W., Yang Y., “Research on selective laser melting of Ti6Al4V: Surface morphologies, optimized processing zone, and ductility improvement mechanism” Metals, Vol. 8, Issue 7, Page 471, 2018.